

Large optical forces on a barium monofluoride molecule using laser pulses for stimulated absorption and emission: A full density-matrix simulation

A. Marsman, D. Heinrich, M. Horbatsch, and E. A. Hessels*

Department of Physics and Astronomy, York University

(EDM³ Collaboration)

(Dated: January 18, 2023)

A full density-matrix simulation is performed for optical deflection of a barium monofluoride (BaF) beam. Pairs of counter-propagating laser pulses are used for stimulated absorption followed by stimulated emission. The scheme produces a force which is nearly an order of magnitude larger than that obtainable using continuous-wave laser deflection, and yields a force-to-spontaneous-decay ratio which is more than an order of magnitude larger. The large reduction in spontaneous decay is key to optical deflection of molecules, where branching ratios to other vibrational states do not allow for cycling transitions. This work is part of an effort by the EDM³ collaboration to measure the electric dipole moment of the electron using BaF molecules embedded in a cryogenic argon solid. Deflection of BaF molecules will separate them from the other ablation products coming from a buffer-gas-cooled ablation source, before embedding them into the argon solid. Our simulations show that sufficiently large deflections for this separation are feasible.

I. INTRODUCTION

Optical forces on atoms produced by laser beams have proven to be an essential tool in atomic physics since they were first suggested [1] and implemented [2]. Most often, these forces result from the absorption of one quantum ($\hbar\vec{k}$) of momentum, followed by a spontaneous decay. This process can lead to a force as large as $F_0 = \hbar k / (2\tau)$, corresponding to a change of one quantum of momentum every two lifetimes.

Alternative atomic laser force schemes use stimulated emission, in which $\hbar\vec{k}$ of momentum is imparted to the atom upon excitation, with a second $\hbar\vec{k}$ added to the atom's momentum by an oppositely-directed laser beam through stimulated emission back down to the ground state. Such stimulated-emission schemes allow for forces larger than F_0 , but at the expense of having to use more complicated setups involving multiple laser beams and time-varying optical fields. One important example of a stimulated-emission force on atoms is the bichromatic force first demonstrated by Grimm, et al. [3] and further developed by others [4–8]. The bichromatic force uses two pairs of counter-propagating laser beams that are offset from each other in frequency. The frequency offset leads to beat notes in both directions, and, at the location of an atom, this beating leads to pulses (offset in time) arriving from each direction.

Another, more straightforward scheme for a stimulated-emission optical force uses pairs of pulses from counter-propagating laser beams to drive stimulated absorption and emission. This scheme has been implemented for atoms by Long, et al. [9]. In the present work, we consider optical forces on molecules and simulate a stimulated-emission scheme that uses laser pulses. We specialize to the barium monofluoride

(BaF) molecule, the molecule being used by the EDM³ collaboration to make an ultraprecise measurement [10] of the electric dipole moment of the electron. For the measurement, BaF molecules produced by a buffer-gas-cooled laser-ablation source are embedded in solid argon. It is necessary to separate the BaF molecules from the other ablation products via a deflection in order to produce an uncontaminated solid. For our geometry, a deflection of nearly 3 m/s (which corresponds to 1000 quanta of photon momentum) is required. This deflection is much larger than demonstrated [11, 12] deflections of other molecules using the bichromatic force.

Molecules present major challenges for optical forces [13]. The first difficulty results from the presence of the vibrational levels. Each time the molecule undergoes a spontaneous emission, it has a branching ratio for returning to a $v > 0$ level of the ground electronic state. For some molecules (including BaF) there are also branching ratios to intermediate electronic states. A set of repump lasers is necessary to return the molecules to the appropriate state if cooling is to continue.

Additionally, for the molecules most suitable for cooling (including BaF), the required transition has a larger number n_g of substates in the ground state compared to the number (n_e) in the excited state. This situation is illustrated in Fig. 1, where the BaF cooling-transition states [14] (the $X^2\Sigma_{1/2} v=0, N=1$ negative parity state and the $A^2\Pi_{1/2} v'=0, j'=1/2$ positive parity state) are shown. Including the hyperfine structure, the ground state consists of $n_g = 12$ substates, whereas the excited state consists of $n_e = 4$ substates. Having $n_g > n_e$ has two adverse effects on laser cooling.

The first effect is that a laser of fixed polarization will quickly pump the population into a dark state (a linear combination of the n_g states that cannot be excited by this polarization), thereby shutting off the optical force. These dark states can be destabilized [15] by, for exam-

* hessels@yorku.ca

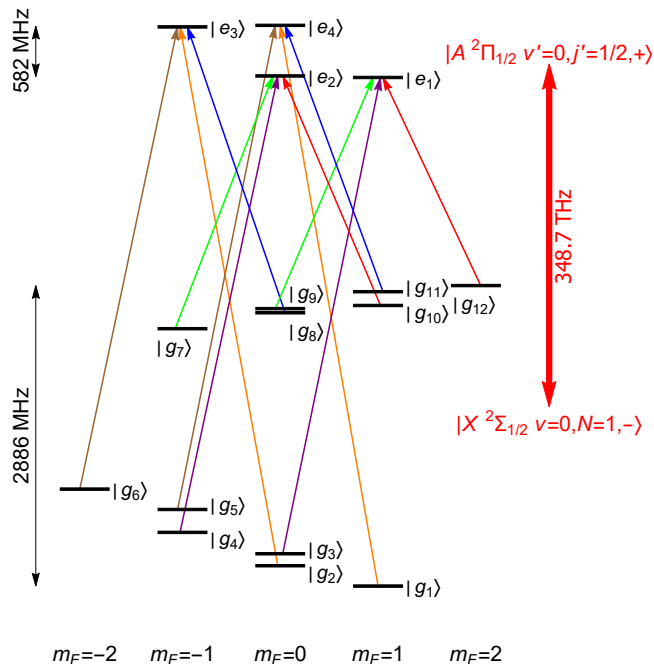


FIG. 1. (color online) The BaF energy levels for the $X^2\Sigma_{1/2}$ $v=0$, $N=1$ negative parity state and the $A^2\Pi_{1/2}$ $v'=0$, $j'=1/2$ positive parity state, with a 1000-gauss magnetic field. The magnetic field resolves individual transitions between substates, and the arrows show the twelve transitions being driven. Due to pairs of similar laser frequencies, these transitions are driven with six laser frequencies, as indicated by the six colors of the arrows and as detailed in Table I.

ple, using a frequency-modulated laser [16] or by using an appropriately-oriented magnetic field [17] which causes the molecules to Larmor precess into bright states. Typically, field strengths on the order of 10 gauss are used for this precession. Our approach for overcoming the dark-state problem is to use a much larger magnetic field (of the order of 1000 gauss) that resolves the individual substates (as shown in Fig. 1) and then to use laser pulses to separately address individual substates.

The second effect of having $n_g > n_e$ is that the force is smaller even when the dark-state problem is addressed. If, for example, there is no dark-state accumulation, and the laser light is effective at equalizing the $n_g + n_e$ state populations, the maximum force possible for a spontaneous-decay force is $F_m = 2F_0 n_e / (n_e + n_g)$. A similar decrease is also found for stimulated-emission forces.

II. OPTICAL DEFLECTION SCHEME

Our proposed scheme for optical deflection uses a series of laser pulses, each with a duration of 2 ns, as shown in Fig. 2(a). A first pulse, from an upward-directed laser beam is immediately followed by a second pulse from a downward-directed beam. The intention is for the first

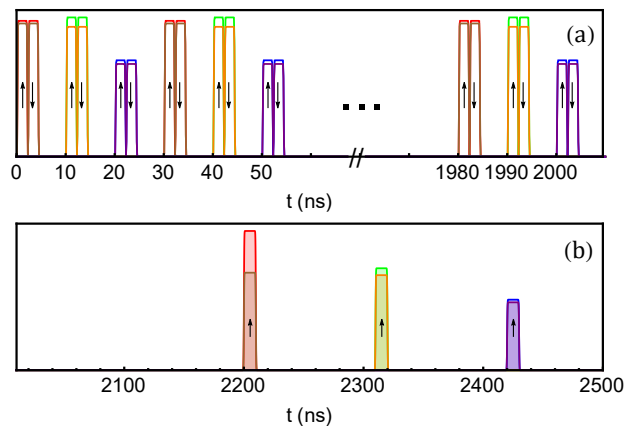


FIG. 2. (color online) The timing diagram for the laser pulses. Panel (a) shows the first 2 μs of deflection. A 2-ns π pulse from the upward-directed laser beam is immediately followed by a similar π pulse from the downward-pointing laser beam. Two frequencies are present in each pulse, as indicated by the colors here and the matching colors in Fig. 1. These two frequencies address populations in four of the twelve $|g_i\rangle$ states. The two pulses are followed 10 ns and 20 ns later by similar pulses that address the other $|g_i\rangle$ states, with this 30-ns sequence being repeated 67 times. After these pulses, single 10.5-ns pulses for each of the analogous laser transitions from the $v=1$ state serve to repump the population back into the $v=0$, as shown in panel (b). The sequence shown in both panels is repeated approximately 15 times during the time the molecule passes through the laser beams.

pulse to move ground-state population up to the excited state, and for the second pulse to stimulate this population back down to the ground state. Each set of two pulses in Fig. 2(a) includes two separate frequencies (as indicated by the two colors of pulses), and these two frequencies drive four transitions, as indicated by the four arrows with these two colors in Fig. 1. A 1000-gauss magnetic field (along the axis of the laser beams) lifts the degeneracies between $|g_i\rangle$ states, allowing these four isolated transitions to be driven, with very little accidental transfer due to other $|g_i\rangle$ -to- $|e_j\rangle$ transitions. The intensities at each frequency are chosen to meet the π -pulse condition, so the population of four of the $|g_i\rangle$ states of Fig. 1 are efficiently excited to the four states, $|e_1\rangle$, $|e_2\rangle$, $|e_3\rangle$ and $|e_4\rangle$, and then returned to the original four $|g_i\rangle$ states.

If the ground state consisted of only four substates, this pair of pulses could be repeated and would lead to two quanta of momentum being imparted during each cycle. With twelve substates, however, spontaneous decay would move population out of these four states into the other eight $|g_i\rangle$ states, and these eight states would be dark states. The dark-state problem can be overcome by having the next pair of pulses (those shown in purple and blue in Fig. 2(a)) address four other $|g_i\rangle$ states using two frequencies that drive the four purple and blue transitions shown in Fig. 1. A third pair of pulses then ad-

addresses the remaining four $|g_i\rangle$ states (orange and brown in Figs. 1 and 2(a)).

If there were no spontaneous decay, this cycle of pulses (the first 30 ns of Fig. 2(a)) could be repeated indefinitely without any concern about dark states. If, however, a spontaneous decay occurs, for example, at 2 ns in Fig. 2(a), the second pulse, which is intended to stimulate the population back down to a $|g_i\rangle$ state would instead excite it up to an $|e_j\rangle$ state, thus imparting a quantum of momentum in the opposite direction. Furthermore, all of the following pulses would similarly perform the reverse role and also impart the wrong sign of momentum to the molecule. In this scenario, the molecule continues to experience this opposite force until another spontaneous decay puts the scheme back on track. The delay time between pulse pairs (e.g., between the pulse centered at 3 ns and the pulse centered at 11 ns in Fig. 2(a)) makes the spontaneous decays that correct the scheme back to the intended cycle happen at a faster rate than spontaneous decays that reverse the force, which can only happen if the spontaneous decay occurs between the closely-spaced pulses (e.g., the pulses centered at 11 and 13 ns in Fig. 2(a)).

The net effect is that most often (about 80% of the time, which comes from the 8-ns center-to-center pulse separation for the delay compared to the 10-ns cycle between pulse pairs) the force is in the correct direction and 20% of the time it is in the wrong direction. This leads to a net force corresponding to 0.6 (80% minus 20%) times two quanta of momentum divided by three per 10 ns. The division by three results from the fact that only one third of the population is addressed during each 10-ns period. The net force predicted is nine times larger than the force F_m possible for spontaneous-decay forces (which could only be achieved if the dark-state problem were eliminated). Compressing the time scale of Fig. 2 would lead to even larger forces, but the shorter pulse duration may require a larger magnetic field to sufficiently resolve the energy levels of Fig. 1 given the broader spectrum inherent in the shortened pulse duration. Higher-intensity laser light would also be needed to satisfy the π -pulse criterion.

As will be seen in the following section, most of the population resides in the ground states at all times. This reduces the spontaneous decays and therefore reduces the population lost to $v = 1$ and other states. As a result, only one repump laser is required in the current scheme.

III. COMPLETE DENSITY-MATRIX SIMULATION

In this section we present a density-matrix simulation of the deflection scheme. Since a BaF molecule in the $A^2\Pi_{1/2}(v=0)$ state has a branching ratio [14] of 96.4% for decay to the $X^2\Sigma_{1/2}(v=0)$ state (see Fig. 3), the sixteen states of Fig. 1 form an almost closed system. However, the 3.5% branching ratio [14] to the $X^2\Sigma_{1/2}(v=1)$

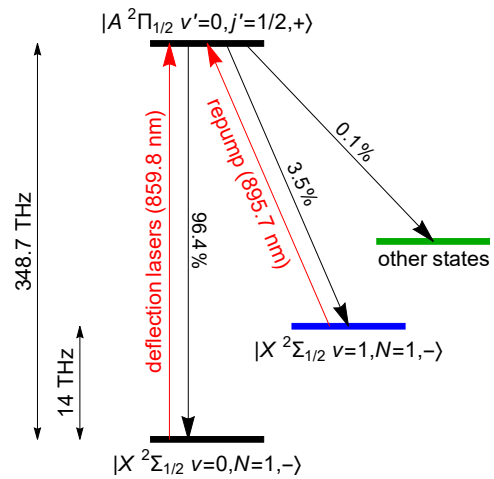


FIG. 3. (color online) The branching ratios for the $A^2\Pi_{1/2}$ state and laser wavelengths needed for our cooling scheme.

state requires an additional twelve ground states ($|g_{13}\rangle$ through $|g_{24}\rangle$) that are the $v = 1$ analogues to $|g_1\rangle$ through $|g_{12}\rangle$ of Fig. 1) to be included in the simulation. A repump laser is required to avoid accumulation of population in these twelve states. The remaining branching ratio of 0.1% [14] includes spontaneous decay to the $X^2\Sigma_{1/2}(v>1)$ states and the $A^2\Delta_{3/2}$ state. Spontaneous decay to the latter state causes the molecule to change its parity upon its second decay down to the $X^2\Sigma_{1/2}$ state. As will be shown, no repump lasers are needed for these states, thus allowing them to be treated as a single additional state ($|g_{25}\rangle$), which acts as a dark state in which population accumulates over time.

In all, 29 states are included in the simulation: 25 ground states and 4 excited states. The time evolution of the density matrix elements can be determined by numerically integrating their differential equations during the time period when the molecule passes through the laser beams:

$$\begin{aligned}
 \frac{d\rho_{gg'}}{dt} &= i\omega_{g'g}\rho_{gg'} + \frac{i}{2} \sum_e (\Omega_{eg'}\rho_{ge} - \Omega_{ge}\rho_{eg'}) \\
 &\quad + \sum_{e,e'} \gamma_{ege'g'}\rho_{ee'}; \\
 \frac{d\rho_{ee'}}{dt} &= i\omega_{e'e}\rho_{ee'} + \frac{i}{2} \sum_g (\Omega_{ge'}\rho_{eg} - \Omega_{eg}\rho_{ge'}) \\
 &\quad - \frac{1}{2} \sum_{g,e''} (\gamma_{ege''g}\rho_{e''e'} + \gamma_{e''ge'g}\rho_{ee''}); \\
 \frac{d\rho_{ge}}{dt} &= i(\omega_{eg} - \omega_v)\rho_{ge} + \frac{i}{2} \sum_{g'} \Omega_{g'e}\rho_{gg'} \\
 &\quad - \frac{i}{2} \sum_{e'} \Omega_{ge'}\rho_{e'e} - \frac{1}{2} \sum_{g',e'} \gamma_{e'g'eg'}\rho_{ge'}, \quad (1)
 \end{aligned}$$

where the indices g and e represent the 25 ground and

4 excited states, respectively. Here, $\hbar\omega_{ab} = E_a - E_b$ is the energy difference between two states $|a\rangle$ and $|b\rangle$, in the 1000-gauss magnetic field. These energies are calculated using the methods detailed in the appendix of Ref. [16] and are listed in Table II in the appendix of this paper. The difference between the average energy of the $|e\rangle$ states and the $|g\rangle$ states for each value of v is denoted by ω_v ($v = 0, 1$). The rotating-wave approximation is used (twice) to avoid the fast oscillations at the optical frequencies ω_0 and ω_1 .

We use the complete formulation for spontaneous decay [18, 19] which includes quantum-mechanical interference from the decay process using

$$\gamma_{ege'g'} = \frac{\omega^3}{3\pi\epsilon_0\hbar c^3} \vec{d}_{ge} \cdot \vec{d}_{e'g'}. \quad (2)$$

The diagonal elements γ_{egeg} are equal to the branching ratio times $1/\tau$. The dipole matrix elements can then be deduced from the measured lifetime of the $A^2\Pi_{1/2}$ state ($\tau = 57.1$ ns [20]), along with the branching ratio [14] to each vibrational state and ratios for transitions from an individual Zeeman state $|e_j\rangle$ to $|g_i\rangle$. These latter ratios are calculated using the methods described in Ref. [16]. The values of the electric dipole matrix elements used are listed in Table III in the appendix.

The Rabi frequencies in Eq. (1) are given by

$$\Omega_{ge}(t) = \vec{d}_{ge} \cdot \sum_p \frac{\hat{\epsilon}_p E_{0p}(\vec{r}, t)}{\hbar} e^{i[(\omega_p - \omega_v)t - \vec{k}_p \cdot \vec{r} + \phi_p]} \Bigg|_{\vec{r}=\vec{r}_m(t)}. \quad (3)$$

Here, \vec{d}_{ge} is the electric dipole matrix element between states g and e and the sum is over all laser fields, which includes the upward and downward beams of Fig. 2(a), with all six frequency components (as detailed in Table I), as well as six repump frequencies, as indicated in Fig. 2(b). The frequencies, wavevectors, phases, polarizations and amplitudes are represented by $\omega_p/(2\pi)$, \vec{k}_p , ϕ_p , $\hat{\epsilon}_p$ and $E_{0p}(\vec{r}, t)$, respectively. The latter includes both the time profile of the laser pulses (Fig. 2) and the spatial profile of the laser beam, which is taken to be a top-hat shape (as, e.g., in Ref. [21]) approximated by an elliptical super-gaussian function of the form

$$e^{(-x^2/w^2 - y^2/h^2)^5}, \quad (4)$$

where the values of w and h are chosen such that the full width at half maximum of the beam is 5 mm in width and 1 mm in height. The values of E_0 used for each of the beams is given in Table I, and these correspond to peak laser powers (during the 2-ns pulses) of approximately 2 W.

Both the \vec{r} dependence in this profile and the \vec{r} in the complex exponential of Eq. (3) are evaluated at the molecular position $\vec{r}_m(t)$. The trajectory of the molecule is obtained from its original position (assumed to be 3.25 mm before the axis of the laser beams), its initial velocity (assumed to be 150 m/s – a typical speed for a BaF

transitions	polarization	Figs. 1&2(a)	Δf (MHz)	E_0 (V/cm)
$ g_{12}\rangle \rightarrow e_1\rangle, g_{10}\rangle \rightarrow e_2\rangle$	σ^-	red	-1696	208
$ g_6\rangle \rightarrow e_3\rangle, g_5\rangle \rightarrow e_4\rangle$	σ^+	brown	+1615	208
$ g_9\rangle \rightarrow e_1\rangle, g_7\rangle \rightarrow e_2\rangle$	σ^+	green	-1659	217
$ g_2\rangle \rightarrow e_3\rangle, g_1\rangle \rightarrow e_4\rangle$	σ^-	orange	+1739	203
$ g_{11}\rangle \rightarrow e_4\rangle, g_8\rangle \rightarrow e_3\rangle$	σ^-	blue	-1104	150
$ g_4\rangle \rightarrow e_2\rangle, g_3\rangle \rightarrow e_1\rangle$	σ^+	purple	+1104	145

TABLE I. The parameters used for the twelve laser transitions of Fig. 1.

molecule in a 4-kelvin helium-buffer-gas-cooled beam [22] – directed towards the axis of the laser beams) and the force obtained [23] from Ehrenfest's theorem:

$$\vec{F}(t) = -\hbar \sum_{e,g} \text{Re}[\rho_{eg}(t) \nabla \Omega_{ge}(\vec{r}, t)] \Bigg|_{\vec{r}=\vec{r}_m(t)}. \quad (5)$$

The density matrix has $29^2 = 841$ components. However, we set $\rho_{gg'} = 0$ when g and g' do not have the same vibrational quantum number v , since the $i\omega_{g'g}$ term in its differential equation causes rotations at an infrared frequency which causes the much slower accumulation in this state from the $\gamma_{ege'g'}$ term to average to zero. The remaining 505 density matrix elements, along with the components of $\vec{r}_m(t)$ and $\dot{\vec{r}}_m(t)$ are numerically integrated over the 45 μ s that it takes for the molecules to pass through the laser profile. These integrations are computationally intensive since the $\omega_{g'g}$ and $\omega_{eg} - \omega_v$ terms in Eq. (1) cause oscillations with periods of less than 1 ns that must be calculated accurately.

The results of this integration are given in Fig. 4, where the total population (red) of the twelve $v=0$ ground states is shown along with the total of the four excited states (blue). The time slice in panel (b) of the figure shows the individual π -pulse population transfers, whereas panel (a) shows time-averaged populations over the time taken by the molecule to pass through the laser beams. On average, only 10% of the population (dashed blue line) is in an excited state, which implies that, on average, it takes approximately ten lifetimes for each molecule to undergo a spontaneous emission. This reduced emission slows the loss of population to dark states; however, by the end of each 2 μ s of deflection laser pulses (Fig. 2(a)), 18% of the population is in the $X^2\Sigma_{1/2} v=1, N=1$ dark states (green in Fig. 4(a)).

To avoid further population buildup in these dark states, six 10.5-ns π pulses (as shown in Fig. 2(b)) drive twelve transitions from each of the twelve $X^2\Sigma_{1/2} v=1, N=1$ states ($|g_{13}\rangle$ through $|g_{24}\rangle$) to one of the $|e_1\rangle$ through $|e_4\rangle$ states. These transitions are the exact $v = 1$ analogues of the transitions shown in Fig. 1 and in Table I, with the longer pulse length compensating for the smaller electric-dipole matrix elements coupling these states. The deflection and repump sequence of Fig. 2 is

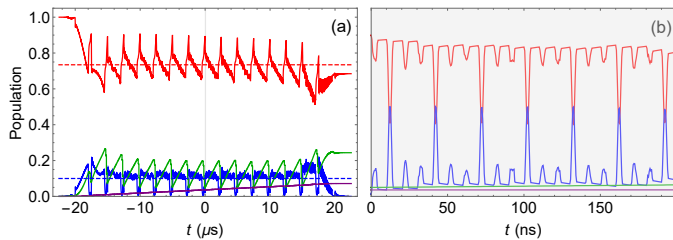


FIG. 4. (color online) The total population of the $v=0$ ground states (red), the excited states (blue), the $v=1$ ground states (green), and all other states (purple). Panel (a) shows the time-averaged (50-ns moving average) populations for the entire deflection time, where it can be seen that the $v=1$ population accumulates to 18% over 2 μs of deflection pulses, at which time repump pulses return the majority to the $v=0$ state. The population in all other states remains small throughout the deflection time indicating that no additional repump lasers are needed. The 200-ns segment shown in the narrow grey region is expanded in panel (b) without time averaging so that the effect of the individual π pulses can be seen. The larger features in this panel are due to excitations from $|g_1\rangle$, $|g_2\rangle$, $|g_7\rangle$, and $|g_9\rangle$, which are the four states with the largest population due to their larger branching ratios.

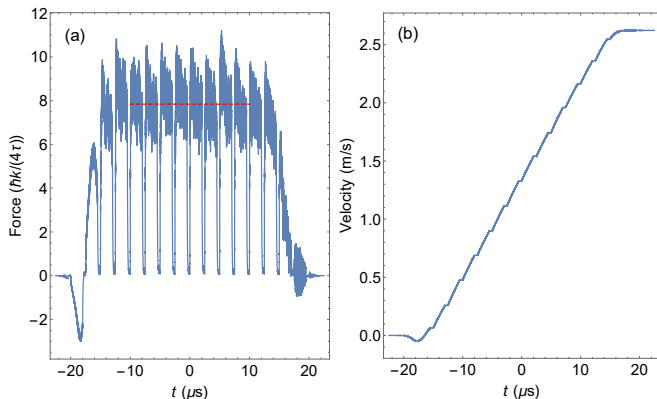


FIG. 5. (color online) The force (a) given in units of F_m and the transverse velocity (b) versus time for a BaF molecule that is being deflected by the scheme presented in this work.

repeated as the molecule passes through the laser beams.

Figure 5(a) shows the force experienced by the molecule as it passes through the laser beam. The average force is eight times larger (dashed line) than the spontaneous-emission force ($F_m = \hbar k / (4\tau)$), showing that our scheme deals effectively with dark states and that the stimulated absorption and emission cycle works almost as efficiently as the estimate given in Section II. This force is significantly larger than demonstrated bichromatic forces on molecules and the simulated [24] bichromatic force on $^{137}\text{Ba}^{19}\text{F}$.

Given the potential loss to dark states for each spontaneous emission, a key figure of merit for molecular deflection is the number of quanta of momentum imparted per spontaneous emission. The combination of the large force

of Fig. 5(a) and the low spontaneous-emission rate due to the low excited-state population of Fig. 4 implies that 20 $\hbar k$ of momentum is imparted per spontaneous decay. This ratio is 20 times larger than that possible for non-stimulated optical deflection schemes. Because of the low level of spontaneous emission, the effect of all of the other dark states (the $|g_{25}\rangle$ state in our model) is minimal, with a population accumulation of less than 5%, as seen by the purple curve in Fig. 4(a). As a result, the present scheme requires only one repump wavelength. In all, two laser wavelengths are required (859.8 and 895.7 nm), each with sidebands to provide six frequencies (see Table I).

Figure 5(b) shows the transverse velocity of the molecule as a function of time. The molecule is deflected by 2.6 m/s as it passes through the lasers. This deflection is sufficient to fully separate BaF molecules from the other ablation products. Since the lasers are only in resonance with the $^{138}\text{Ba}^{19}\text{F}$ isotope, the resulting BaF beam will be isotopically pure.

An important practical consideration for any deflection scheme is the dependence of the deflecting force on the laser parameters, which are bound to be imperfectly set in an actual implementation of the deflection. Full density matrix simulations are repeated multiple times with the six values of E_0 of Table I (and the similar six values for the $v = 1$ transitions) individually multiplied by random factors between 0.95 and 1.05. These simulations show that the deflection is robust against variations of the laser field amplitude, with the standard deviation of the resulting deflections (σ_{defl}) being less than 2%. Similarly, imperfect polarization for each of the 18 different laser pulses (differing in frequency or direction) is modelled by replacing σ^\pm polarization in Table I with $\sigma^\pm + \epsilon\sigma^\mp$, where ϵ is chosen randomly to be between -1% and $+1\%$ for each laser. The deflection was also robust against this variation, with a standard deviation σ_{defl} of less than 1%. Finally, the phase of all eighteen laser frequencies was randomly varied (between 0 and 2π) and again the variation in deflection was small, with $\sigma_{\text{defl}} < 6\%$.

The simulations were also performed with different initial velocities. Changing the longitudinal component of the velocity along the molecular beam axis has only a small effect on the magnitude of the force. For example, a 7% change in this longitudinal component leads to a change in the force of less than 2%. We also repeated the simulations with different initial velocity components transverse to the molecular beam axis (along the axis of the laser beams), while fixing the longitudinal component at 150 m/s. In order to separate the BaF molecules from the other ablation products, we need only to communicate to transverse velocity components of between -2 and $+2$ m/s. However, the simulations show that our deflection scheme is effective over a wide range of transverse speeds, as shown in Fig. 6.

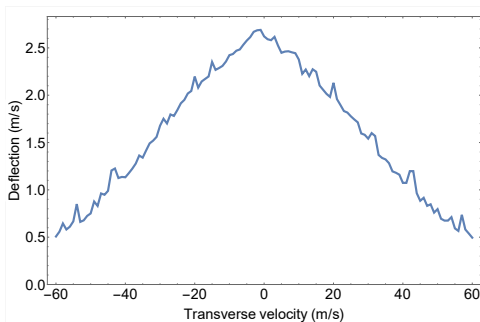


FIG. 6. (color online) Deflection of the BaF molecule versus its initial transverse velocity. The scheme described in this work is effective over a large velocity range.

IV. CONCLUSIONS

In this work, we have performed a complete density-matrix simulation of a scheme that is capable of providing strong laser deflection forces for molecules. Pairs of pulses from oppositely-directed laser beams are used to stimulate population to an excited state followed by stimulated emission. Dark states are avoided by applying a magnetic field large enough to resolve transitions between individual magnetic substates. This scheme would allow for a beam of $^{138}\text{Ba}^{19}\text{F}$ to be separated from other laser

ablation products coming from a buffer-gas-cooled laser-ablation source, as required by the EDM³ collaboration for their planned measurement of the electric dipole moment of the electron using BaF molecules embedded in an Ar solid.

V. ACKNOWLEDGEMENTS

We acknowledge support from the Gordon and Betty Moore Foundation, the Alfred P. Sloan Foundation, the John Templeton Foundation (through the Center for Fundamental Physics at Northwestern University), the Natural Sciences and Engineering Council of Canada, the Canada Foundation for Innovation, the Ontario Research Fund and from York University. Computations for this work were enabled by support provided by the Digital Research Alliance of Canada, Compute Ontario and SHARCNET.

APPENDIX

The energies of the $v = 0$ states shown in Fig. 1 were calculated using the methods detailed in Ref. [16], as were the electric-dipole matrix elements between these states. The calculated energies are listed in Table II, and the electric-dipole matrix elements are listed in Table III.

-
- [1] A. Ashkin, Acceleration and trapping of particles by radiation pressure, *Phys. Rev. Lett.* **24**, 156 (1970).
 - [2] R. Schieder, H. Walther, and L. Wöste, Atomic beam deflection by the light of a tunable dye laser, *Optics Communications* **5**, 337 (1972).
 - [3] R. Grimm, Y. B. Ovchinnikov, A. I. Sidorov, and V. S. Letokhov, Observation of a strong rectified dipole force in a bichromatic standing light wave, *Phys. Rev. Lett.* **65**, 1415 (1990).
 - [4] J. Söding, R. Grimm, Y. B. Ovchinnikov, P. Bouyer, and C. Salomon, Short-distance atomic beam deceleration with a stimulated light force, *Phys. Rev. Lett.* **78**, 1420 (1997).
 - [5] M. R. Williams, F. Chi, M. T. Cashen, and H. Metcalf, Measurement of the bichromatic optical force on Rb atoms, *Phys. Rev. A* **60**, R1763 (1999).
 - [6] M. R. Williams, F. Chi, M. T. Cashen, and H. Metcalf, Bichromatic force measurements using atomic beam deflections, *Phys. Rev. A* **61**, 023408 (2000).
 - [7] M. Partlow, X. Miao, J. Bochmann, M. Cashen, and H. Metcalf, Bichromatic slowing and collimation to make an intense helium beam, *Phys. Rev. Lett.* **93**, 213004 (2004).
 - [8] M. A. Chieda and E. E. Eyler, Bichromatic slowing of metastable helium, *Phys. Rev. A* **86**, 053415 (2012).
 - [9] X. Long, S. Y. Scarlett, A. M. Jayich, and W. C. Campbell, Suppressed spontaneous emission for coherent momentum transfer, *Phys. Rev. Lett.* **123**, 033603 (2019).

g	m_F	E_g (MHz)	e	m_F	E_g (MHz)
1	1	-1464.63	1	1	-292.14
2	0	-1431.73	2	0	-289.66
3	0	-1412.34	3	-1	289.65
4	-1	-1377.77	4	0	292.16
5	-1	-1340.75			
6	-2	-1307.81			
7	-1	1351.63			
8	0	1377.39			
9	0	1384.07			
10	1	1389.16			
11	1	1411.43			
12	2	1421.34			

TABLE II. The relative energies of the ground states $|g\rangle$ and excited states $|e\rangle$ of Fig. 1 for a 1000-gauss magnetic field.

- [10] A. C. Vutha, M. Horbatsch, and E. A. Hessels, Orientation-dependent hyperfine structure of polar molecules in a rare-gas matrix: A scheme for measuring the electron electric dipole moment, *Phys. Rev. A* **98**, 032513 (2018).
- [11] I. Kozyryev, L. Baum, L. Aldridge, P. Yu, E. E. Eyler, and J. M. Doyle, Coherent bichromatic force deflection of molecules, *Physical Review Letters* **120**, 063205 (2018).

σ^-			π			σ^+		
e	g	$\langle e d g\rangle$	e	g	$\langle e d g\rangle$	e	g	$\langle e d g\rangle$
2	1	-0.015	1	1	-1.329	1	2	-0.001
4	1	0.963	2	2	-1.329	1	3	-1.350
3	2	0.964	4	2	-0.005	2	4	1.350
3	3	-0.016	2	3	0.0004	4	4	-0.028
3	8	1.285	4	3	0.030	2	5	-0.034
3	9	0.259	3	4	-0.031	4	5	-0.939
2	10	-0.939	3	5	-0.015	3	6	0.940
4	10	-0.016	3	7	1.328	2	7	-0.909
2	11	0.006	2	8	0.023	4	7	-0.016
4	11	-1.312	4	8	0.262	1	8	-0.194
1	12	0.940	2	9	0.010	1	9	0.888
			4	9	-1.302			
			1	10	0.016			

TABLE III. The electric-dipole matrix elements between the states of Fig. 1 (in units of ea_0) for a magnetic field of 1000 gauss, which defines the quantization axis. The non-zero $\Delta m_F = 0$ (π) and $\Delta m_F = \pm 1$ (σ^\pm) matrix elements are shown. The similar matrix elements connecting to the $v = 1$ states are smaller by a factor of $\sqrt{0.035/0.964}$.

- [12] S. E. Galica, L. Aldridge, D. J. McCarron, E. E. Eyler, and P. L. Gould, Deflection of a molecular beam using the bichromatic stimulated force, *Phys. Rev. A* **98**, 023408 (2018).
- [13] N. J. Fitch and M. R. Tarbutt, Laser-cooled molecules, *Advances in Atomic, Molecular, and Optical Physics* **70**, 157 (2021).
- [14] Y. Hao, L. F. Pařteka, L. Visscher, P. Aggarwal, H. L. Bethlem, A. Boeschoten, A. Borschevsky, M. Denis, K. Esajas, S. Hoekstra, and K. Jungmann, High accuracy theoretical investigations of CaF, SrF, and BaF and implications for laser-cooling, *J. Chem. Phys.* **151**, 034302 (2019).
- [15] D. J. Berkeland and M. G. Boshier, Destabilization of dark states and optical spectroscopy in Zeeman-degenerate atomic systems, *Phys. Rev. A* **65**, 033413 (2002).
- [16] P. Kaebert, M. Stepanova, T. Poll, M. Petzold, S. Xu, M. Siercke, and S. Ospelkaus, Characterizing the Zeeman slowing force for $^{40}\text{Ca}^{19}\text{F}$ molecules, *New Journal of Physics* **23**, 093013 (2021).
- [17] E. S. Shuman, J. F. Barry, and D. DeMille, Laser cooling of a diatomic molecule, *Nature* **467**, 820 (2010).
- [18] D. Cardimona and C. Stroud Jr, Spontaneous radiative coupling of atomic energy levels, *Phys. Rev. A* **27**, 2456 (1983).
- [19] A. Marsman, M. Horbatsch, and E. A. Hessels, Shifts due to distant neighboring resonances for laser measurements of 2^3S_1 -to- 2^3P_j transitions of helium, *Physical Review A* **86**, 040501 (2012).
- [20] P. Aggarwal, V. R. Marshall, H. L. Bethlem, A. Boeschoten, A. Borschevsky, M. Denis, K. Esajas, Y. Hao, S. Hoekstra, K. Jungmann, and T. B. Meijknecht, Lifetime measurements of the $A^2\Pi_{1/2}$ and $A^2\Pi_{3/2}$ states in BaF, *Phys. Rev. A* **100**, 052503 (2019).
- [21] H. Ma, Z. Liu, P. Jiang, X. Xu, and S. Du, Improvement of Galilean refractive beam shaping system for accurately generating near-diffraction-limited flattop beam with arbitrary beam size, *Optics Express* **19**, 13105 (2011).
- [22] S. Truppe, M. Hambach, S. M. Skoff, N. E. Balleid, J. S. Bumby, R. J. Hendricks, E. A. Hinds, B. E. Sauer, and M. R. Tarbutt, A buffer gas beam source for short, intense and slow molecular pulses, *J. Modern Optics* **65**, 648 (2018).
- [23] R. J. Cook, Atomic motion in resonant radiation: An application of Ehrenfest's theorem, *Phys. Rev. A* **20**, 224 (1979).
- [24] F. Kogel, M. Rockenhäuser, R. Albrecht, and T. Langen, A laser cooling scheme for precision measurements using fermionic barium monofluoride ($^{137}\text{Ba}^{19}\text{F}$) molecules, *New Journal of Physics* **23**, 095003 (2021).